



저작자표시-비영리-변경금지 2.0 대한민국

이용자는 아래의 조건을 따르는 경우에 한하여 자유롭게

- 이 저작물을 복제, 배포, 전송, 전시, 공연 및 방송할 수 있습니다.

다음과 같은 조건을 따라야 합니다:



저작자표시. 귀하는 원저작자를 표시하여야 합니다.



비영리. 귀하는 이 저작물을 영리 목적으로 이용할 수 없습니다.



변경금지. 귀하는 이 저작물을 개작, 변형 또는 가공할 수 없습니다.

- 귀하는, 이 저작물의 재이용이나 배포의 경우, 이 저작물에 적용된 이용허락조건을 명확하게 나타내어야 합니다.
- 저작권자로부터 별도의 허가를 받으면 이러한 조건들은 적용되지 않습니다.

저작권법에 따른 이용자의 권리는 위의 내용에 의하여 영향을 받지 않습니다.

이것은 [이용허락규약\(Legal Code\)](#)을 이해하기 쉽게 요약한 것입니다.

[Disclaimer](#)

공학석사학위논문

**LES 를 이용한 항공기 와후류의
Crow 불안정성에 관한 연구**

**Parametric Study of Crow Instability in Aircraft
Wake Vortices Using Large Eddy Simulation**

2018 년 2 월

서울대학교 대학원
기계항공공학부
박 준 민

LES 를 이용한 항공기 와후류의 Crow 불안정성에 관한 연구

Parametric Study of Crow Instability in Aircraft
Wake Vortices Using Large Eddy Simulation

지도교수 이 관 중

이 논문을 공학석사 학위논문으로 제출함

2018 년 2 월

서울대학교 대학원

기계항공공학부

박 준 민

박준민의 공학석사 학위논문을 인준함

2017 년 12 월

위 원 장

李 樹 甲 

부위원장

李 贊 中 

위 원

金 奎 弘 

초 록

항공기 와후류는 쉽게 소산되지 않고 일정 시간 대기 중에 머무르는 성질이 있다. 와후류의 거동 및 소산은 Crow 불안정성 (Crow instability) 이라고 불리는 현상과 밀접한 연관이 있음이 알려져 있으며, 평행한 한 쌍의 와후류가 불안정성 영향으로 만나 고리를 형성하며 소산되는 과정이 특징적이다. 때문에 비행기로부터 발생한 한 쌍의 와후류 소산 과정이 대기조건에 따라 어떻게 달라지는지에 대한 연구가 그간 이루어져왔다. 그러나 공항이 운용됨에 있어서 평행한 활주로에서의 횡풍에 의한 와후류 이동, 향로 교차에 의한 두 쌍의 와후류가 상호작용하는 거동 및 소산이 발생할 가능성이 있으나, 아직 이와 관련한 연구는 부족하다. 이에 본 연구에서는 한 쌍의 와후류가 단독으로 거동했을 때와, 와후류 쌍이 다른 와후류 쌍과 상호 영향을 주고 받으며 거동할 때의 차이를 LES 난류모델을 이용해 해석하였다. 와후류는 항공기 최대이륙질량에 따라 소형(light), 중형(medium), 및 대형(heavy) 급 항공기의 와후류 매개변수를 선정하여 Burnham-Hallock 모델로 모사하였다. 그 결과 소형-중형 상호작용 시 두 쌍의 와후류 수명이 모두 짧아지는 것을 확인하였다. 또한 중형-중형 상호작용 시 와후류가 합쳐지며 순환이 일시적으로 강해졌다가 소산되는 것이 확인되었으며, 중형-대형 상호작용 시 대형 항공기 와후류가 단독 거동 와후류 대비 약 5배 빠르게 연결되는 결과가 나타났다. 대형 항공기에 의한 와후류가 순환 강도가 크고, 오랜 시간동안 그

강도가 유지되기 때문에 중형-대형 상호작용의 결과는 공항의 활주로 이용 효율을 높이기 위한 이·착륙 분리간격 조정 시 반영이 가능할 것으로 판단된다.

주요어 : 항공기 와후류, Crow 불안정성, 와후류 간 상호작용, 대기 난류 강도, 대와류모사 (LES)

학 번 : 2016-20739

ABSTRACT

Parametric Study of Crow Instability in Aircraft Wake Vortices Using Large Eddy Simulation

Joonmin Park

Mechanical and Aerospace Engineering

The Graduate School

Seoul National University

Aircraft wake vortices are not easily dissipated so they stay in the atmosphere for a certain period of time. It is known that the transport and decay of wake vortices are closely related to the phenomenon called Crow instability. A parallel pair of wake vortices links due to the long-wave sinusoidal instability, and forms a ring while dissipating rapidly. To predict the behavior of wake vortices, research has been conducted dealing with the effect of atmospheric conditions such as eddy dissipation rate, and stratification level. In various conditions, only a single pair of wake vortices was superimposed to the computational domain. However, there is a possibility of interactions among vortices where runways are parallel so that a pair of vortices from an aircraft moves to another runway path due to crosswind. In addition, the interaction can happen where the flight paths are crossing each other, so it is necessary to analyze the difference between the behavior of a pair of wake vortices and the

transport and decay of two pairs of wake vortices. In this paper, parametric study of aircraft wake vortices are conducted using large eddy simulation (LES) turbulence model. Vortex parameters were selected for light, medium, and heavy aircraft and the velocity distribution of a vortex was modeled using Burnham-Hallock vortex model. As a result, it was confirmed that the vortex lifespan was shortened in light – medium interaction. In medium – medium interaction case, the circulation strength became temporarily stronger as vortices were combined and then they were dissipated. It was also found that in medium – heavy interaction case, the linking of vortices from heavy aircraft happened 5 times faster than the case of a single pair of vortices from heavy aircraft without interaction. Since the vortices from large aircraft have high circulation which maintains for a long time, the results from medium – heavy interaction case can be reflected to the adjustment of separating interval between airplanes to improve airport efficiency.

keywords : Wake Vortices, Crow Instability, Interaction Among Vortices, Large Eddy Simulation (LES)

Student Number: 2016-20739

Table of Contents

국 문 초 록.....	i
ABSTRACT.....	iii
Table of Contents	v
List of Figures	vi
1. Introduction	1
2. Numerical Simulations.....	7
2.1. Governing Equations and Numerical Methods.....	9
2.2. Initial Conditions and Boundary Conditions.....	12
2.2.1. Stochastic Noise Generation and Radiation (SNGR) and Forcing Technique	12
2.3. Vortex Parameters	17
3. Results and Discussion.....	19
3.1. Crow Instability for General Cases.....	19
3.2. Parametric Study of Two Pairs of Vortices: Crow Instability	26
3.2.1. Single Pair of Vortices	29
3.2.2. Interaction Between Two Pairs of Vortices.....	33
4. Conclusions	41
Appendix A. Crow Instability Visualization by Han et al. [6]	43
Appendix B: The Simplified Model from De Visscher et al. [9]	44
References	46

List of Figures

Fig. 1 Possible encounters with lift-generated wake by a following aircraft; V. J. Rossow [4].....	2
Fig. 2 Instability of a pair of trailing vortices of a B-47 aircraft photographed at intervals of 15 s after its passage; Van Dyke [11]	4
Fig. 3 Situation example where crossing of aircraft vortices can occur behind an aircraft; NATS Services [14]	6
Fig. 4 Flow chart for wake vortex analysis	8
Fig. 5 Forcing technique to make background turbulence field	14
Fig. 6 Spatial distribution of the turbulent velocity field generated by SNGR; velocity vector is plotted in the x-z plane	14
Fig. 7 Spatial distribution of the turbulent velocity field right before the vortices are injected; velocity vector is plotted in the x-z plane	14
Fig. 8 Time evolution of turbulent kinetic energy (TKE) before vortices are injected	16
Fig. 9 Top and side views of wake vortices at three different nondimensional times for the case of weak ($\varepsilon^* = 0.0789$) and strong ($\varepsilon^* = 0.5844$) turbulence intensities.....	22
Fig. 10 Averaged total circulation, lateral spacing, and vertical displacement of vortices.....	25
Fig. 11 Initial condition for analyzing interaction among vortices	28
Fig. 12 Top views of wake vortices at three different nondimensional times for the cases of light, medium, and heavy aircraft	31
Fig. 13 The evolution of averaged vortex circulation and vertical position with respect to aircraft MTOW	32

Fig. 14 Isometric view of light – medium wake vortices interaction at three different times 35

Fig. 15 Averaged lateral separation, vertical position, circulation with respect to t^* and top-view snapshot at $t^* = 4.86$ of medium wake vortices interacted with light and without interaction 35

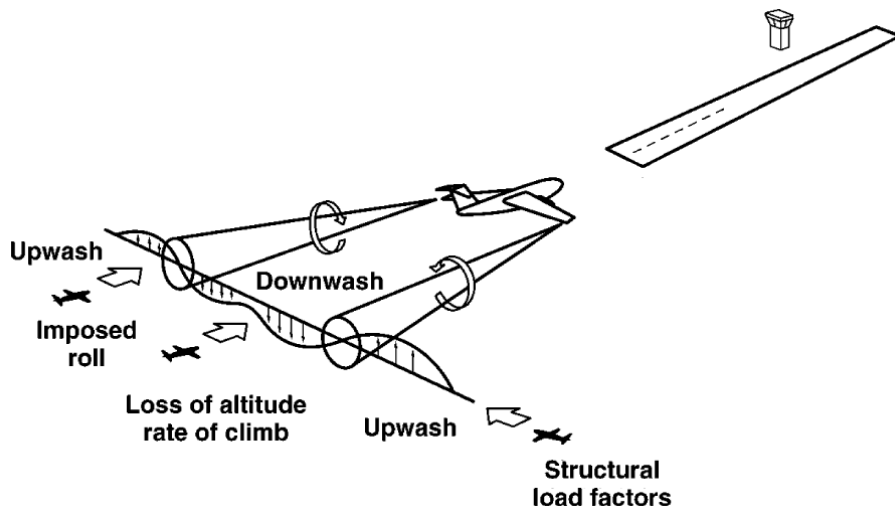
Fig. 16 Averaged lateral separation, vertical position, circulation of wake vortices from medium sized aircraft with respect to t^* and snapshots at four different times 38

Fig. 17 Top views and isometric views at two different time and averaged circulation of wake vortices of heavy aircraft with respect to t^* interacted with vortices from medium one and without interaction..... 40

Fig. 18 Top and side views of wake vortices at three different nondimensional times for the case of weak ($\epsilon^* = 0.0789$) and strong ($\epsilon^* = 0.5844$) turbulence intensities..... 43

1. Introduction

Wake vortices are formed mainly at the wingtip of an aircraft because of pressure difference between the upper and the lower part of the wing. Vortices are rolled up to a single pair of counter rotating ones. The initial lateral separation, b_0 , of vortices is about 70-80% length of the wingspan [1]. Due to the rolling moment generated by the wake vortices, a following aircraft may lose its controllability and descend abruptly, or even may crash into the ground (Fig. 1). It is reported that the incidents caused by wake vortices occur frequently during approach to the airport or low altitude flight [2]. For example, in January 2008, Air Canada A319 dived 1,400 feet with maximum of 55° rolling because of the wake vortices from B747-400 which was flying 11 NM ahead. The carts used for in-flight meal ran up to the ceiling and fell off, causing passengers to be injured. In order to prevent such accidents, the International Civil Aviation Organization (ICAO) and the Federal Aviation Administration (FAA) have designated separation intervals according to the size difference between the leading aircraft and the following one, so that the aircraft can be operated safely [3].



**Fig. 1 Possible encounters with lift-generated wake by a following aircraft;
V. J. Rossow [4]**

Meanwhile, in order to cope with the increasing air traffic, there has been a growing interest in improving the capacity of the airport by adjusting the interval between aircraft during take-off and landing. The aircraft is classified into four categories based on the maximum take-off mass (MTOM). Those are A380-800, heavy (136,000 kg or more), medium (7,000 kg or more and 136,000 kg or less) and light (7,000 kg or less). However, in the medium class for example, the difference between the maximum value and the minimum value is significant, which is about 130 t. It means that there can be difference of up to 130 t among medium class aircraft. In other words, if considering two different airplanes categorized as a medium aircraft, for example, A320 and ERJ-145, are following the heavy class aircraft A340-600, setting gaps with the preceding aircrafts as 5 NM can be too conservative for the A320.

Therefore, research about re-categorizing the current classification more specifically is on the way at the moment [5]. It is also possible to increase the aircraft capacity by constructing another runway to airports, but it is limited because of problems such as securing site, and cost needed to build one. Therefore, in order to adjust the separation that is empirically set at the moment, it is necessary to study the transport and decay of the wake vortices from an aircraft.

The transport and decay of vortices are closely related to the surrounding atmospheric conditions such as turbulence intensity (ϵ) and stratification level [6]-[9]. Vortices show long-wave symmetric sinusoidal instability, which is also known as Crow instability [10], and the evolution of the instability is dependent of the atmospheric conditions. The parallel pair of vortices change their patterns due to Crow Instability and create a continuous vortex-ring like a train (Fig. 2). The time taken for making a ring is called the vortex lifespan and vortices dissipate rapidly after the formation of the ring. This phenomenon is named after Crow who identified it firstly.

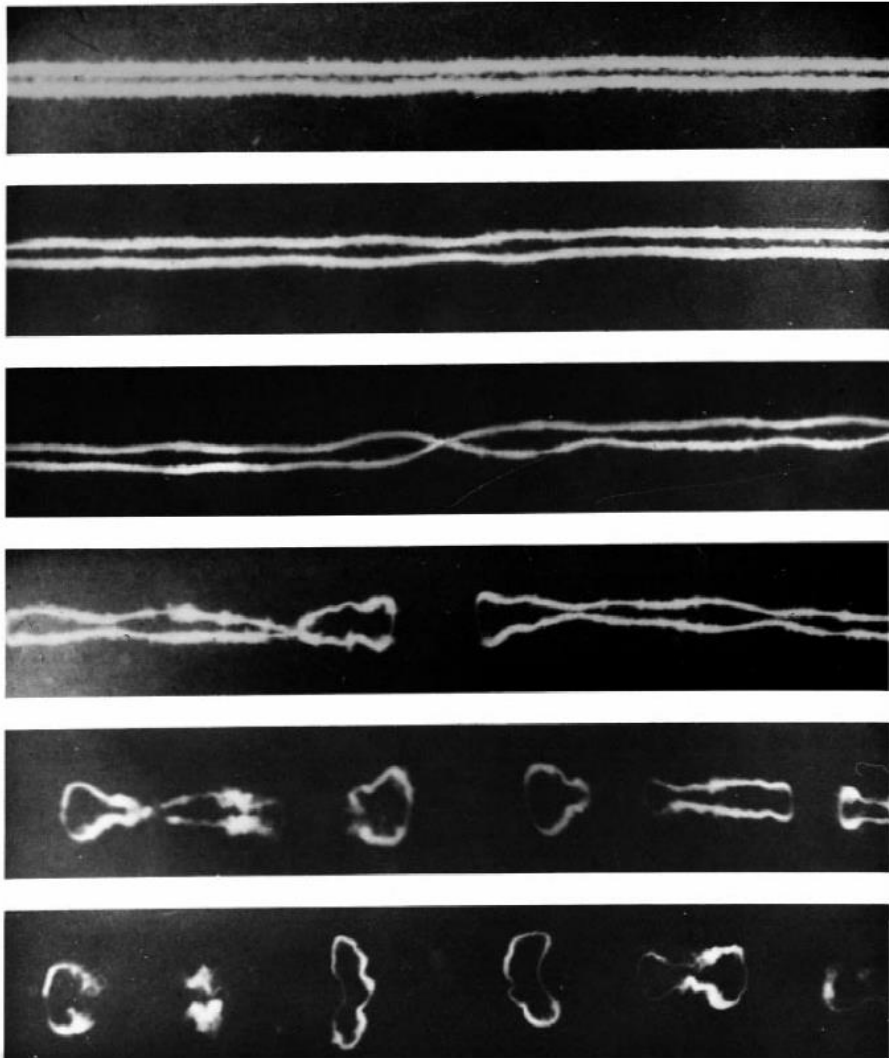


Fig. 2 Instability of a pair of trailing vortices of a B-47 aircraft photographed at intervals of 15 s after its passage; Van Dyke [11]

Crow and Bate have found that the life span of vortices is a function of the non-dimensional turbulence intensity [12]. In addition, Sarpkaya and Daly showed that the non-dimensional descent distance of vortices is a function of the dimensionless time, turbulence intensity, and the longitudinal integral length scale [13]. Based on these studies, Han et al. [6] analyzed the influence of the turbulence intensity on the development of Crow Instability using the LES simulation. They found that the maximum amplified wavelength of instability and the vortex lifespan decrease as dimensionless turbulence intensity increases excluding the effects of stratification level.

Recently, the influence of atmospheric stratification level on the Crow instability of aircraft wake vortices has been analyzed using LES [7]–[9]. If the stratification level is low or moderate, the development of Crow instability is promoted. Contrarily, at high stratification level, it is found that the instability of short wavelength is developed dominantly so the wake vortices are rapidly dissipated.

In the previous studies, only a pair of vortices was examined with various atmospheric conditions as mentioned above. However, considering the environment of an airport (Fig. 3), it is possible that a pair of vortices is generated in the atmosphere where another pair of vortices from the preceding aircraft still exists. For example, runways are parallel so that a pair of vortices from an aircraft moves to another runway path due to crosswind. In addition, the flight paths may cross each other. In such cases, the vortices of the following aircraft are influenced by interacting with the other vortices remained in the atmosphere. Therefore, it is necessary to clarify the transport

and decay mechanism of the vortices considering the interaction with another pair of vortices.

In this study, we investigated the difference in the behavior of vortices between when they are generated in a calm atmosphere and when they are interacted with vortices from another aircraft. The validity of the LES simulation was confirmed by comparing the results to a previous study under same conditions. The results of present study are expected to be useful for adjusting the interval between aircraft during the take-off and landing. Section 2 describes the LES model and the methods for numerical simulations. Section 3 provides a comparative analysis with previous studies for code verification, and the results and analysis of present study on the interaction of two pairs of vortices. Finally, Section 4 draws conclusion.

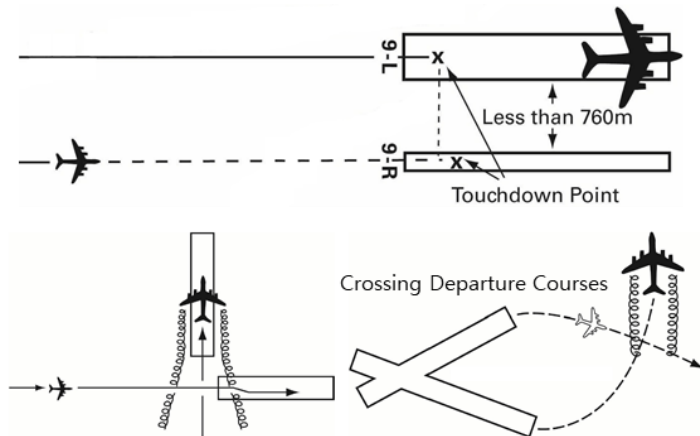


Fig. 3 Situation example where crossing of aircraft vortices can occur behind an aircraft; NATS Services [14]

2. Numerical Simulations

The overall flow of the simulation is described in the Fig. 4. First, we set the computational domain and generate the grid. Since the behavior of wake vortices varies depending on the atmospheric conditions, it is essential to make atmospheric background turbulence under specific conditions. In order to create a flow field with eddy dissipation rate similar to a real atmospheric condition, stochastic noise generation and radiation (SNGR) and forcing technique are used. In this process, the LES simulation continues and the statistical steady-state isotropic turbulence is generated as background turbulence. After the background turbulence is generated, a pair of counter-rotating vortices with same magnitude of circulation is modeled and added to the flow field. Then LES simulation is continuously performed to observe the behavior of vortices over time. When interpreting the behavior of a pair of vortices alone, the LES simulation is performed for the desired time and the procedure goes to the post-processing. On the other hand, when observing the interaction between two pairs of wake vortices, another pair of vortices is added to the flow field during the LES simulation. After that, the LES simulation is conducted for the required time (dotted line in Fig. 4). In the next section, each procedure is being explained in more detail starting from governing equations and numerical methods.

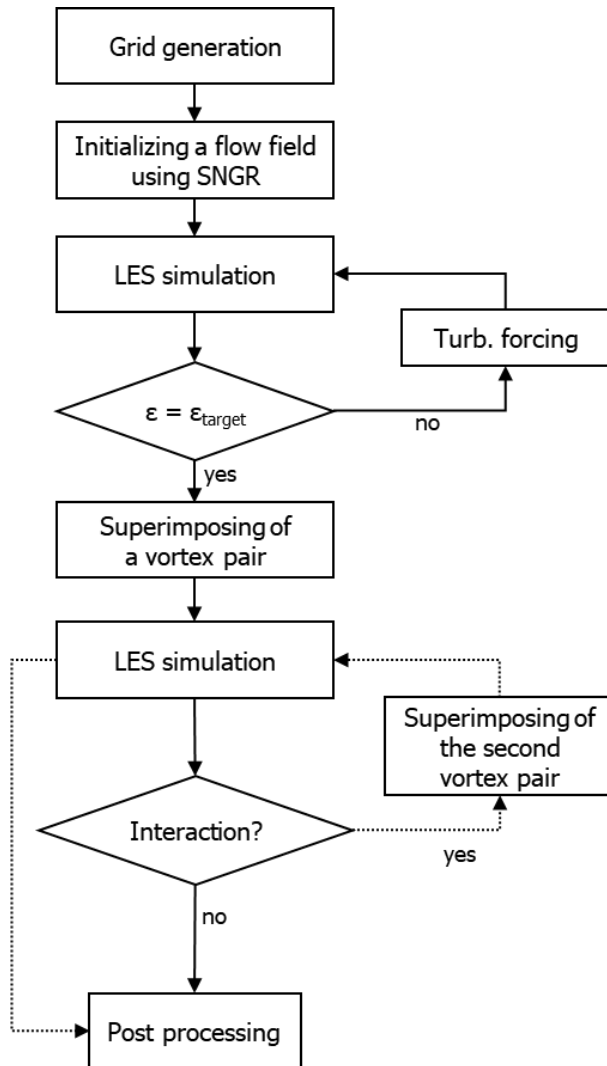


Fig. 4 Flow chart for wake vortex analysis

2.1. Governing Equations and Numerical Methods

The basic equations for CFD analysis are three-dimensional compressible Navier-Stokes (N-S) equations as follows:

$$\begin{aligned}\frac{\partial \rho}{\partial t} + \frac{\partial \rho u_j}{\partial x_j} &= 0 \\ \frac{\partial \rho u_i}{\partial t} + \frac{\partial \rho u_i u_j}{\partial x_j} + \frac{\partial p}{\partial x_i} &= \frac{\partial \sigma_{ij}}{\partial x_j} \\ \frac{\partial \rho E}{\partial t} + \frac{\partial (\rho E + p) u_j}{\partial x_j} &= \frac{\partial \sigma_{ij} u_i}{\partial x_j} - \frac{\partial}{\partial x_j} q_j\end{aligned}\quad (1)$$

where u_i is the direction component of velocity, t is time, ρ is density, p is pressure, σ_{ij} is stress tensor, and q_j is heat flux. Grid filtering and Favre filtering are used for LES simulation. Unresolved quantity and filtered value are expressed with superscript and overbar, respectively on Eq. (2). In addition, Favre-filtered value is expressed with tilde on the top of variables.

$$\begin{aligned}f &= \bar{f} + f' \\ \tilde{f} &= \frac{\overline{\rho f}}{\bar{\rho}}\end{aligned}\quad (2)$$

Then the final equations of system consist of filtered continuum equation, momentum equation, and energy equation as below.

$$\begin{aligned} \frac{\partial \bar{\rho}}{\partial t} + \frac{\partial}{\partial x_j} (\bar{\rho} \tilde{u}_j) &= 0 \\ \frac{\partial}{\partial t} (\bar{\rho} \tilde{u}_i) + \frac{\partial}{\partial x_j} (\bar{\rho} \tilde{u}_i \tilde{u}_j + p^+ \delta_{ij}) &= \frac{\partial \tau_{ij}^+}{\partial x_j} + \frac{\partial}{\partial x_j} (\mu \tilde{S}_{ij}) \\ \frac{\partial}{\partial t} (\bar{\rho} \tilde{e}_t) \frac{\partial}{\partial x_i} [(\bar{\rho} \tilde{e}_t + p^+) \tilde{u}_i] &= \frac{\partial Q_i}{\partial x_i} + \frac{\partial}{\partial x_i} \left(k \frac{\partial T}{\partial x_i} \right) + \frac{\partial}{\partial x_i} (\mu \tilde{u}_j \tilde{S}_{ij}) \quad (3) \end{aligned}$$

Smagorinsky model is used for sub-grid scale model. In Smagorinsky model, turbulent eddy viscosity (ν_t) is represented like Eq. (4).

$$\nu_t = (C_s \Delta)^2 \sqrt{2S_{ij}S_{ij}} \quad (4)$$

Smagorinsky constant C_s is selected to be 0.16. S_{ij} , the rate-of-strain tensor is $S_{ij} = 1/2(\partial u_i/\partial x_j + \partial u_j/\partial x_i)$. Δ is a criterion related to the size of grid and LES filtering, which is defined as $\Delta = (\Delta x \times \Delta y \times \Delta z)^{1/3}$. In order to accurately describe the isotropy characteristic of small eddies, the grid size is made smaller than the integral length scale, L_{11} . The integral length scale can be calculated by Eq. (5) where the domain averaged value is denoted by $\langle \cdot \rangle$.

$$L_{11} = \int_0^{\infty} \langle u(x)u(x+r) \rangle / \langle u^2 \rangle dr \quad (5)$$

LES is based on the code that is collaborated with Tohoku University. The accuracy of the solver was confirmed using Doswell's frontogenesis model [15], [16]. Other details for numerical simulations are given in Table 1.

The length of the calculation area in the axial direction, which is parallel to the aircraft heading, is set to be larger than 8 times of the initial lateral separation of vortices to observe the most amplified wavelength (MAW) of Crow instability.

Table 1 Flow simulation methods

Inviscid numerical flux	Roe's flux difference splitting method using a higher-order monotonic upwind scheme for conservation laws (MUSCL) scheme ^[17]
Viscous term	2 nd -order central difference
Time integration	4 th -order Runge-Kutta method
Turbulence model	LES (Smagorinsky model)

2.2. Initial Conditions and Boundary Conditions

It is necessary to generate an initial background turbulence in order to see the characteristics of the wake vortices according to the atmospheric conditions. In order to generate the initial flow field, SNGR method was used. In addition, forcing technique was implemented to adjust the eddy dissipation rate as in realistic atmospheric conditions. Periodic boundary conditions are applied for all directions. The influence of the boundary conditions is negligible because the vertical computational domain is four times as high as the initial spacing of the wake vortices. Moreover, it is advantageous to simulate the behavior of wake vortices for a long time by applying the periodic boundary conditions.

2.2.1. Stochastic Noise Generation and Radiation (SNGR) and Forcing Technique

First, SNGR model [18] was used to generate random turbulence. In the model, the random velocity field $\mathbf{u}_t(\mathbf{x})$ is defined as a finite sum of discrete Fourier modes as in Eq. (6):

$$\mathbf{u}_t(\mathbf{x}) = 2 \sum_{n=1}^N \tilde{u}_{tn} \cos(\mathbf{k}_n \cdot \mathbf{x} + \Psi_n) \boldsymbol{\sigma}_n \quad (6)$$

where \mathbf{x} is a position vector, and \tilde{u}_{tn} , Ψ_n , σ_n are the n^{th} mode components of the wave vector \mathbf{k}_n , indicating the amplitude, phase, and direction, respectively.

In the case of random turbulence generated by SNGR, it can be seen that the velocity distribution is symmetrical about the middle point as shown in Fig. 6. SNGR is expressed mathematically as homogeneous isotropic turbulence, but it is different from actual atmospheric turbulence. Therefore, for the more accurate atmospheric turbulence simulation, a method of artificially adding external force to the low-frequency wave component of the flow field has been adopted [19]. Three-dimensional fast Fourier transform (FFT) of the flow field is conducted at each time step, and then a fixed amplitude f is added to the wave number whose magnitude is less than 3.0 [6],[9]. Finally, the inverse fast Fourier transform (inverse FFT) was performed (Fig. 5). Since the size of computational domain is not same for x , y , and z direction, the actual wavelength along the longitudinal, transverse and vertical directions can be calculated differently. In this case, the components in the longest direction are normalized with respect to the shortest direction, so that energy is not added to waves of different sizes according to the directions, but added to waves of the same size for each direction.

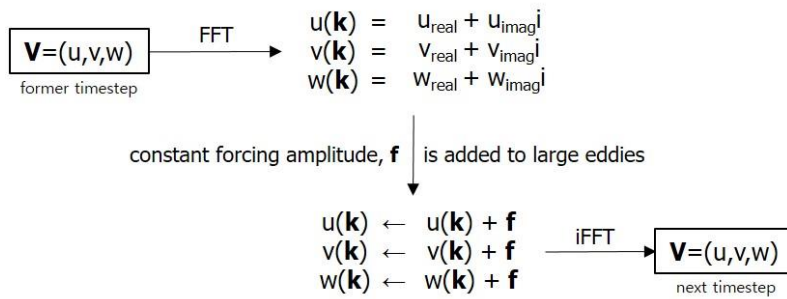


Fig. 5 Forcing technique to make background turbulence field

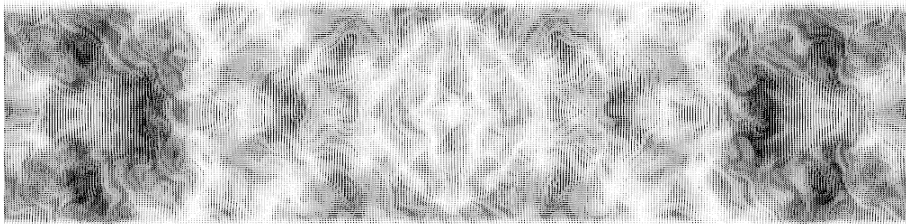


Fig. 6 Spatial distribution of the turbulent velocity field generated by SNGR; velocity vector is plotted in the x-z plane

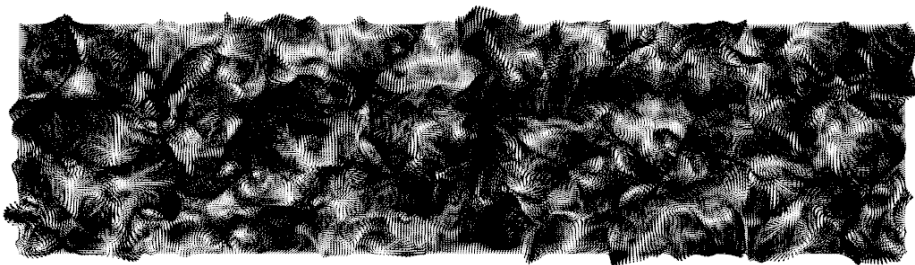


Fig. 7 Spatial distribution of the turbulent velocity field right before the vortices are injected; velocity vector is plotted in the x-z plane

Since the low-frequency component exhibits the longest wavelength characteristic, adding energy here can be regarded as adding the flow components of large eddies from a physical point of view. This added components transfer energy to the small eddies according to the energy cascade of the turbulence, which eventually leads to turbulent dissipation by viscosity. Therefore, the turbulent field reaches a statistical steady state when the energy added and the energy dissipated by the viscosity become equal.

Fig. 8 shows that the turbulent flow field enters the statistical steady state after about 400 seconds. At this time, if the integral length scale L_{11} according to Eq. (5) is calculated, it is confirmed that $L_{11} = 11$ m. In addition, isotropy parameters that are defined as Eq. (7) and Eq. (8), both I_1 and I_2

$$I_1 = [\langle u^2 \rangle / \langle v^2 \rangle]^{0.5} \quad (7)$$

$$I_2 = [\langle w^2 \rangle / \langle v^2 \rangle]^{0.5} \quad (8)$$

oscillate around 1. Since the isotropic parameters in the isotropic turbulence field are 1, it can be confirmed that the generated turbulence field is the isotropic turbulence field.

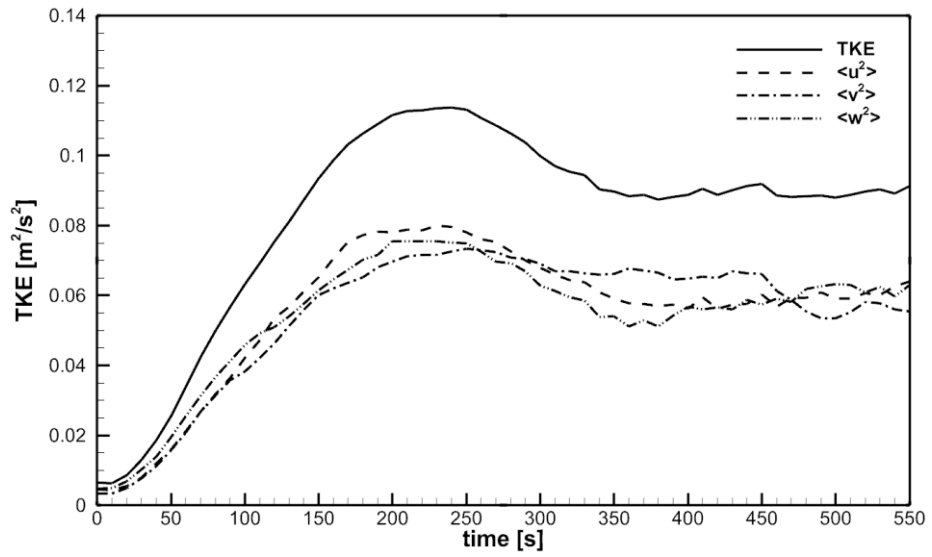


Fig. 8 Time evolution of turbulent kinetic energy (TKE) before vortices are injected

2.3. Vortex Parameters

It is generally known that vortex core radius, r_c is usually $r_c = 0.05b_0$. However, since Crow instability is not significantly influenced by r_c / b_0 [10], the core radius is set to satisfy $\Delta < r_c / 3$ to precisely predict the physics of wake vortices [9].

In case of wake vortex, the post roll-up wake vortex was assumed after the aircraft passed. The distribution of the tangential velocity $V_\theta(r)$ at a distance r away from the center of the vortex core was calculated using the Burnham-Hallock vortex model [20]. The Burnham-Hallock vortex model is widely used for applications such as aircraft wake vortex initialization and the simulating of aircraft behavior near wake vortices. The tangential velocity distribution is expressed by the following equation.

$$V_\theta(r) = \frac{\Gamma_0}{2\pi r} \times \frac{r^2}{r^2 + r_c^2} \quad (9)$$

In Eq. (9), Γ_0 is the initial circulation of the vortex, r is the distance from the center, and $V_\theta(r)$ has the maximum value at the vortex nucleus radial position, $r = r_c$. In case of the initial circulation, it can be calculated through the Eq. (10) as a function of the aircraft mass (M) and wingspan (b).

$$\Gamma_0 = 4Mg/\pi\rho Vb \quad (10)$$

By Biot-Savart law, the wake vortices initially fall at the rate of $V_0 \simeq \Gamma_0/2\pi b_0$. V_0 and b_0 can be used to define the dimensionless time $t^* = t/t_0$ ($t_0 = b_0/V_0$) and the dimensionless turbulence intensity $\varepsilon^* = (\varepsilon b_0)^{1/3}/V_0$.

3. Results and Discussion

The results are divided into two parts. First, a general one pair of wake vortices behavior is examined, and then the results are to be verified by comparing them to those of previous research. The second part of the paper is about the behavior of wake vortices under the interaction with other wake vortices.

3.1. Crow Instability for General Cases

First, it is a part for comparison and validation of codes. The behavior of post roll-up vortices with respect to nondimensional turbulence intensity is described. The initial conditions are same with those of Han et al. [6] and the results from the paper are in appendix A.

The grid size is set to $324 \times 128 \times 128$ and the grid size is $(\Delta x, \Delta y, \Delta z) = (1.0 \text{ m}, 0.66 \text{ m}, 0.66 \text{ m})$. The initial lateral separation of vortices is $b_0 = 16 \text{ m}$. We set the domain length to be long enough in the axial direction to simulate the maximum amplification wavelength of Crow instability. In addition, the length in the transverse direction and the vertical direction corresponds to $5b_0$, which limits the influence of the boundaries. The vortex core radius, r_c , is set to 2 m , and statistical steady state isotropic turbulence is generated using the SNGR and forcing technique. Then, a pair of counter-

rotating wake vortices with opposite circulation is generated in the flow field.

The λ_2 -criterion proposed by Jeong and Hussain [21] is used to visualize the vortex behavior. λ_2 is the second eigenvalue of $S_2 + \Omega_2$, where S and Ω are the strain-rate tensor (symmetric part) and the spin tensor (antisymmetric part) of the velocity gradient tensor ($\nabla\mathbf{u}$), respectively.

$$S_{ij} = \frac{1}{2} \left(\frac{\partial u_i}{\partial x_j} + \frac{\partial u_j}{\partial x_i} \right), \quad \Omega_{ij} = \frac{1}{2} \left(\frac{\partial u_i}{\partial x_j} - \frac{\partial u_j}{\partial x_i} \right) \quad (11)$$

The λ_2 -criterion is widely used in computational fluid dynamics because it has a merit of expressing high shear. Where the value of λ_2 is negative has a vortex flow. The wake vortices can be visualized by the iso-surface of λ_2 . The results are expressed using the top view and the side in Fig. 9.

As a result, it can be seen that the nondimensional time t^* required for the linking of wake vortices is reduced as the dimensionless turbulence intensity ε^* increases. This is in accordance with the results by Han et al. [6] as well as other previous studies [9]. With weak turbulence intensity, it clearly shows the formation of a vortex ring which results from Crow instability. In addition, it has almost symmetrical shape with respect to the x axis without advection effect by the atmospheric turbulence. However, under strong turbulent conditions, it is difficult to observe the formation of the ring, and the asymmetrical behavior of the pair of wake vortices with respect to x -axis is confirmed. This is because the atmospheric turbulent intensity is stronger than

the circulation strength of the wake vortices, so that the interactions with atmospheric turbulence are more prominent than Crow instability.

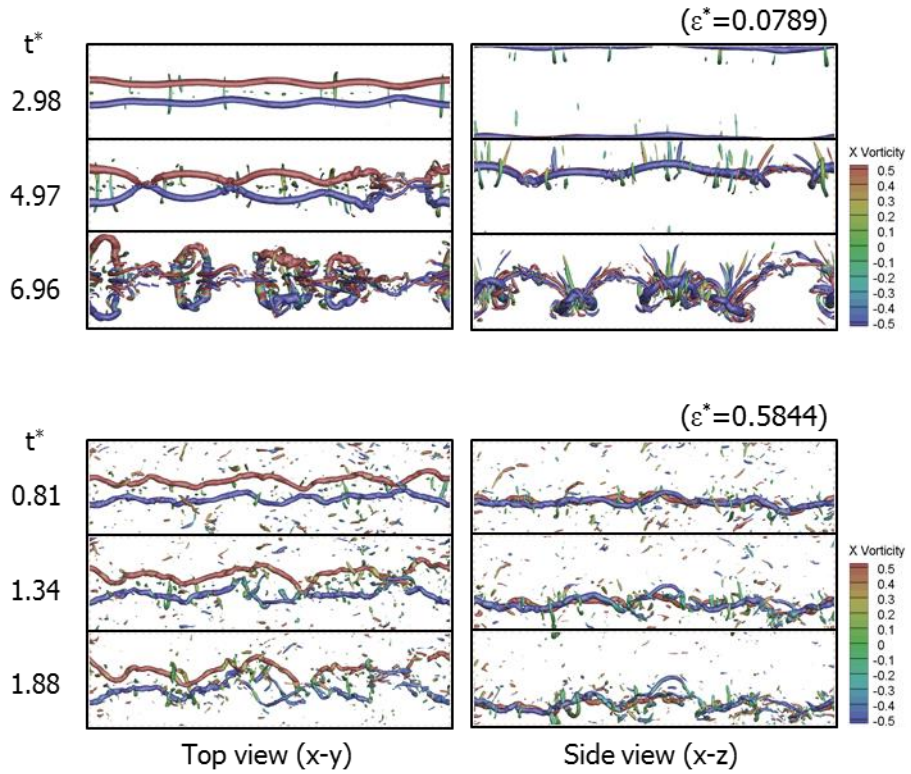


Fig. 9 Top and side views of wake vortices at three different nondimensional times for the case of weak ($\varepsilon^* = 0.0789$) and strong ($\varepsilon^* = 0.5844$) turbulence intensities

In addition, in all cross sections with respect to x-axis, we can find the position of the center of vortex core by finding the position with the largest vorticity within the calculation region. After finding the position of the vortex core center for each section, it can be averaged as Eq. (12) and Eq. (13).

$$\bar{y}(t) = \frac{1}{n_x} \sum_{i=0}^{n_x-1} y(x_i, t) \quad (12)$$

$$\bar{z}(t) = \frac{1}{n_x} \sum_{i=0}^{n_x-1} z(x_i, t) \quad (13)$$

In particular, in the case of the vertical position, the rate of change of the vertical position with time can be modeled as shown in Eq. (14), considering the induced velocity by the Biot-Savart law between the counter-rotating vortices.

$$\frac{dz^*}{dt^*} = v_{BS}^* = -\Gamma_{tot}^* \quad (14)$$

As shown in Fig. 10, since there is no stratification level due to the potential temperature difference, the vertical position calculated by Biot-Savart law alone is in good agreement with the LES results.

Similarly, the value when the circulation becomes maximum according to the distance from the position of the vortex center in each x cross section is defined as $\Gamma_{tot}(x, t) = \max \Gamma(x, r, t)$. The averaged total circulation value can also be defined as Eq. (15).

$$\bar{\Gamma}_{tot}(t) = \frac{1}{n_x} \sum_{i=0}^{n_x-1} \Gamma_{tot}(x_i, t) \quad (15)$$

It can be nondimensionalized by Γ_0 and the evolution of it is in Fig. 10. Two-phase decay is shown. In the first phase, the circulation intensity does not substantially decrease before the vortices form a ring. The second phase begins with the formation of a ring due to Crow instability. The larger the dimensionless turbulence intensity, the faster the point becomes. This is consistent with previous studies and De Visscher's model [9] (detailed formulas are listed in the appendix B) can be applied to explain the results

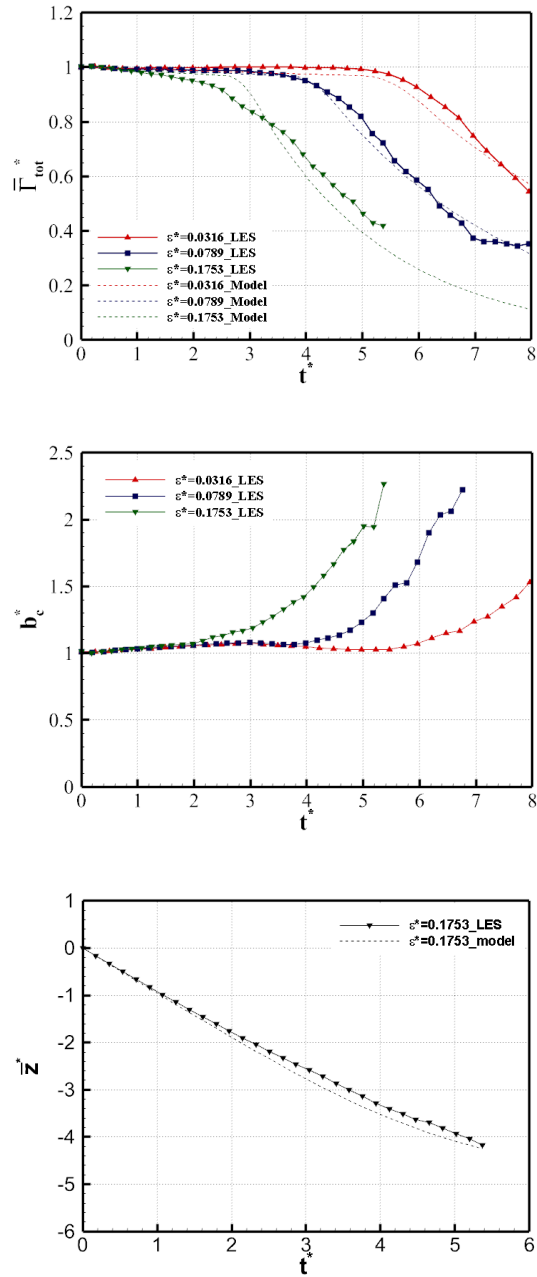


Fig. 10 Averaged total circulation, lateral spacing, and vertical displacement of vortices

3.2. Parametric Study of Two Pairs of Vortices: Crow Instability

In this section, it will be discussed that the difference in the behavior of a pair of wake vortices between itself alone and when it is interacting with other wake vortices. As in Section 3.1, a pair of post roll-up vortices was simulated using Burnham-Hallock vortex model. The number of grids was $360 \times 360 \times 120$ and the grid size was $\Delta = 0.89$ m. The initial lateral separation of vortices and the circulation strength were set as shown in Table 2, according to the size of the aircraft. The vortex core radius was set to $r_c = 2.8$ m, and statistical steady state isotropic turbulence was generated using the SNGR and forcing technique. Then, a pair of counter-rotating vortices with same circulation strength was superimposed in the flow field. In order to confirm the effect of the interaction, the results of a pair of wake vortices alone are shown in 3.2.1. In 3.2.2., an interaction effect will be explained. In cases where interaction happens, a pair of wake vortices is added and after a certain time, another pair of wake vortices is superimposed to the field (Fig. 11). Light-medium, medium-medium, and medium-heavy combinations are selected as the cases for confirming the interaction effects. The time difference applied between the firstly added vortices and the secondly superimposed vortices is half of the current separation time ruled by the ICAO. This is arbitrarily set by assuming that the aircraft wake vortices move to other places because of various factors such as crosswind, or the crossing of the flight path resulting in the interaction among vortices. To compare the effect of interaction with the cases without interaction, results of a single pair of vortices are to be described firstly.

Table 2 Vortex parameters for different aircraft sizes

	Light	Medium	Heavy
Γ_0 [m ² /s]	45	265	400
b_0 [m]	16	27	40
Model example	Business jet	A320, B737	DC-10, B747

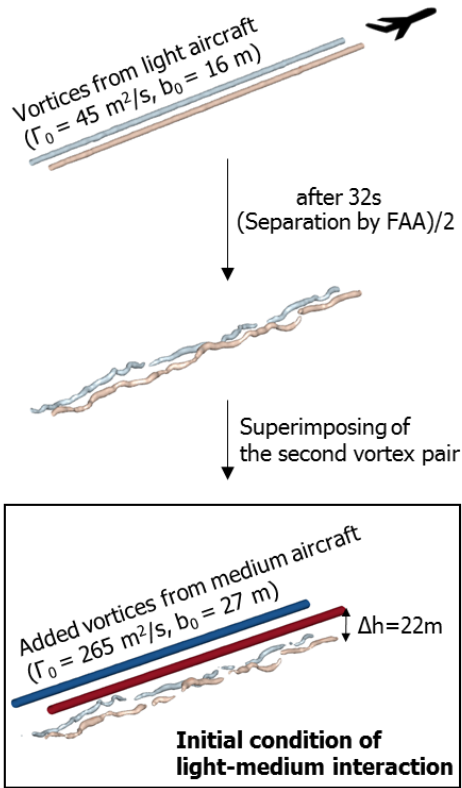


Fig. 11 Initial condition for analyzing interaction among vortices

3.2.1. Single Pair of Vortices

The results of LES simulation of the wake vortices for each aircraft size are present in this section. In the case of vortices from light aircraft, the atmospheric turbulence intensity is relatively stronger than the initial circulation strength of vortices. The dimensionless turbulence intensity is calculated as $\varepsilon_{\text{light}}^* = 0.355$. Therefore, the formation of a ring is not clearly visible, and the irregular distortion of wake vortices due to atmospheric advection effect is observed (Fig. 12).

In the case of wake vortices from medium aircraft or heavy aircraft, the initial circulation intensity is larger than the one from light aircraft. The dimensionless turbulence intensities are calculated as $\varepsilon_{\text{medium}}^* = 0.121$ and $\varepsilon_{\text{heavy}}^* = 0.135$, respectively. In other words, the circulation intensity is relatively stronger than the atmospheric turbulence intensity compared to $\varepsilon_{\text{light}}^*$. Therefore, the formation of a vortex ring resulting from the Crow instability is clearly observed. In addition, secondary vortices are generated over time by three-dimensional interaction between the wake vortices and atmosphere.

As shown in Fig. 13, the non-dimensional vortex lifespan, which represents the time until the linking happens decreases with increasing dimensionless turbulence intensity as in previous studies (Fig. 13). The actual circulation intensity of vortices from light aircraft however, is only about 11% of that of the heavy aircraft. Therefore, it has little effect on the trailing aircraft. In the case of wake vortices from medium aircraft, the non-dimensional circulation seems to maintain for a longer period than that from the heavy aircraft, but the

actual value is about 60% of that from heavy aircraft.

The difference in the characteristics of vortices from each aircraft is also evident in the descending speed due to induced effect (Fig. 13). Vortices from light aircraft has a descending speed of about 0.45 m/s, which is about 30% of that from medium and heavy aircraft, 1.6 m/s. Therefore, it can be seen that if the vortices from lighter aircraft are located higher than the vortices from heavier airplane, there is a greater likelihood that the interaction will not occur due to the difference in descent speed. Considering this, interaction cases are chosen such that the vortices from the relatively light aircraft are located at lower position, and the vortices from the relatively heavy aircraft are at higher position. In the next section, we will look at the mechanism by which the two pairs of vortices meet and interact.

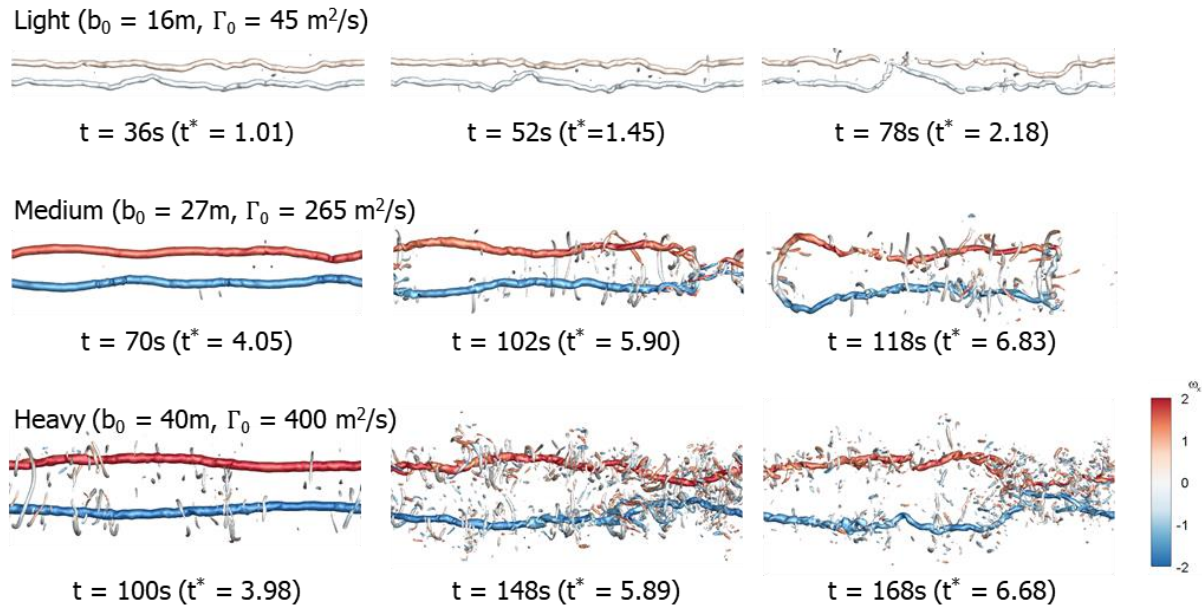


Fig. 12 Top views of wake vortices at three different nondimensional times for the cases of light, medium, and heavy aircraft

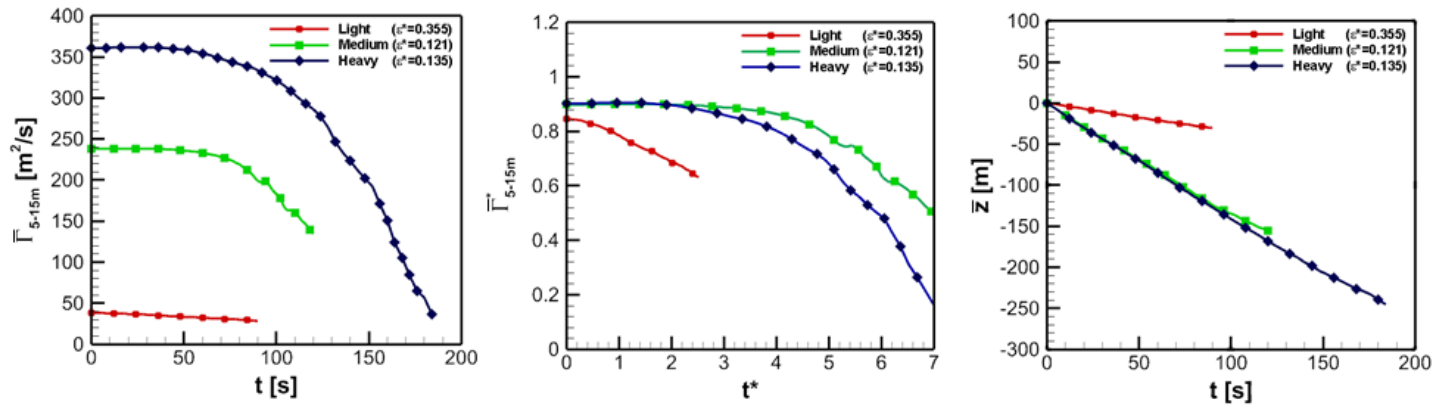


Fig. 13 The evolution of averaged vortex circulation and vertical position with respect to aircraft MTOW

3.2.2. Interaction Between Two Pairs of Vortices

As the first case considering interaction, a pair of wake vortices from light aircraft and that from medium aircraft is considered. The vortices from the medium aircraft were formed 22 m higher than the other one, and 32 s after the vortices from light aircraft were generated. The circulation strength of vortices from light aircraft is small compared to the atmospheric turbulence intensity, so vortices are distorted by the atmospheric advection effect. In addition, the descending speed is about 0.45 m/s, which is smaller than the descending speed of vortices from medium aircraft of 1.6 m/s. Therefore, the vortices generated by medium aircraft move quickly to the position where vortices formed by light aircraft are and the interaction occurs. It is shown that the vortices generated from the light aircraft disappeared due to the strong induced velocity of the vortices made by medium aircraft (Fig. 14).

Although vortices from light aircraft dissipate quickly, there is also an impact on the vortices from medium aircraft (Fig. 15). At the beginning, the lateral separation of the vortices from medium aircraft is slightly reduced by the induced effect of vortices from light aircraft. In addition, the slope of the time-vertical position graph shows that the descent rate also becomes slightly higher. At the same time, the circulation intensity is slightly increased as the vortices from medium aircraft reach the vertical position of the vortices from light aircraft. Once the circulation is added, the vortices from medium aircraft make the vortices from light aircraft dissipate. As a result, it can be seen that secondary vortices are generated more compared to the case when just a

single pair of wake vortices from medium aircraft is considered. Secondary vortices accelerate dissipation by interacting with the primary vortices. Therefore, it can be seen that the vortices interacted with the other ones from light aircraft show an earlier linking compared to the vortices without interaction. After the linking, the circulation strength of vortices from medium aircraft interacted with those from light aircraft is always lower than the case when just a pair of wake vortices from medium aircraft is considered.

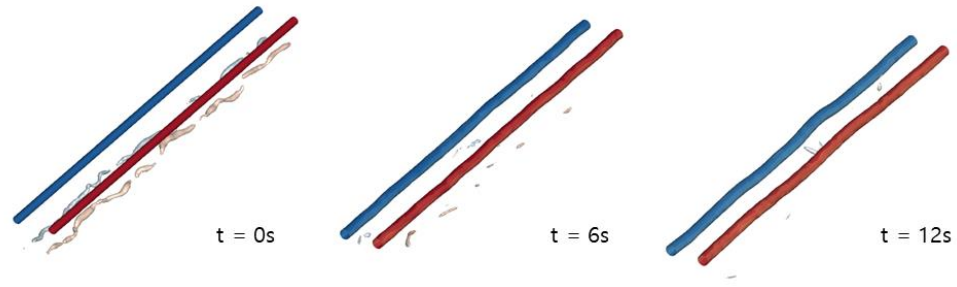


Fig. 14 Isometric view of light – medium wake vortices interaction at three different times

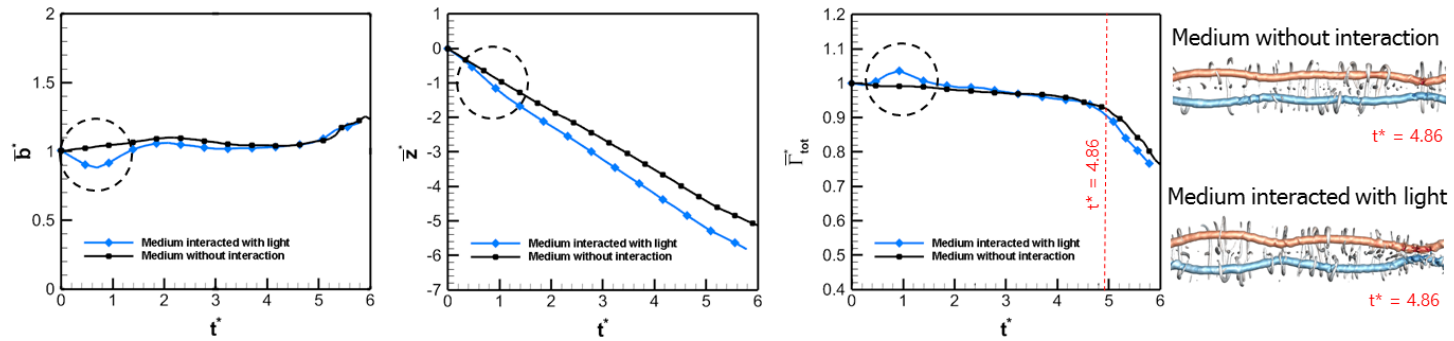


Fig. 15 Averaged lateral separation, vertical position, circulation with respect to t^* and top-view snapshot at $t^* = 4.86$ of medium wake vortices interacted with light and without interaction

The second case is where interactions among vortices from medium aircraft such as B737 have occurred. 38 s after the generation of the vortices by the preceding aircraft, a pair of vortices from another medium aircraft was formed at 27 m higher. Before $t^* = 0.58$, the wake vortices formed at higher position move downward while gathering to the center by the induced effect of the vortices at lower part (Fig. 16). The vortices located at lower position are being separated with a relatively low descent rate. As a result, it can be seen that at $t^* = 0.58$, the vortices of the trailing aircraft are gathered to $0.45b_0$ compared to the initial gap b_0 . Meanwhile, the vortices of the preceding aircraft is about $1.6b_0$ away from each other. In addition, at this point, there is a vertical stoppage of the vortices from preceding aircraft. This is because the descent due to the induced velocity of vortices from the preceding aircraft has been canceled by the ascent due to the induced velocity of vortices from the trailing aircraft. On the other hand, vortices from the trailing aircraft go down at a faster rate than when they are acting alone. The reason is that the descent due to the induced velocity of vortices from the trailing aircraft is combined with the descent due to the induced velocity of the vortices from the preceding aircraft.

After $t^* = 0.58$, there is a phenomenon opposite to that of the previous time because of the position change between two pairs of vortices. In other words, the vortices from trailing aircraft that has descended with high speed while gathering toward each other before are being spread on both sides, and the descending speed of them becomes small. As the vortices from preceding aircraft which have been separated away and have maintained its altitude before on the other hand, the descending speed gradually increases. This is

also due to the superposition effect of mutual induction, which can be concatenated with the results before $t^* = 0.58$. The vortices at higher position are gathered close to each other and have a higher descending speed, whereas the vortices at lower position are spread on both sides and have a lower descending speed.

It is confirmed that a pair of vortices (marked in red in Fig. 16) starts merging together as they change their vertical positions again at $t^* = 1.39$. Over time, the two vortices are rolled-up together in more parts and are observed to be combined about half the length at $t^* = 1.62$. In addition, at this point, linking occurs with the vortices rotating the other way (marked in blue in Fig. 16). It is clearly observed that the circulation intensity decreases after the connection happens. The vortex lifetime is reduced to about one-third compared to the case of single pair of vortices from medium aircraft.

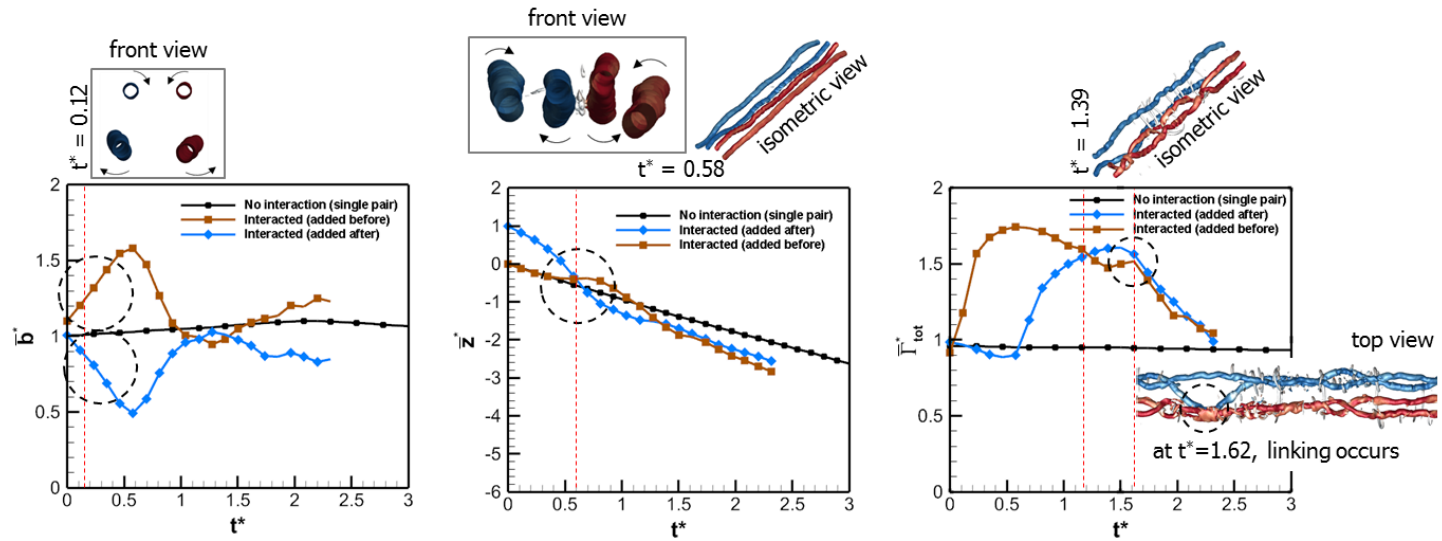


Fig. 16 Averaged lateral separation, vertical position, circulation of wake vortices from medium sized aircraft with respect to t^* and snapshots at four different times

The last is the case where a pair of vortices from heavy aircraft such as the DC-10, A340, or B747 is generated with a height difference of 33 m, and 38 s after the vortices from medium aircraft are formed. As in the previous case, the induced effect of the vortices from medium aircraft makes the vortices from large aircraft move closer. The induced effect of the vortices from large aircraft on the other hand, causes the vortices from medium aircraft to separate in the opposite direction. Up to this point, there seems to be no distinct differences from the previous cases. However, a characteristic phenomenon appears at $t^* = 0.8$ as the vortices from heavy aircraft get close enough for linking to be occurred (Fig. 17). As the vortices from heavy aircraft are getting closer, the circulation strength of them becomes smaller. At $t^* = 1.03$, the linking point is fully attached and the circulation strength decreases by about 20 %. Considering that the time required to reduce the circulation strength to 50 % is about $t^* = 6$ in the case of single pair of vortices from heavy aircraft, the dissipation of the vortices from heavy aircraft interacted by those from medium aircraft can be seen to be very rapid. As vortices from heavy aircraft have a significant impact on airport operations in a view of vortex separation minima, the result of this case shows the possibility of reducing the separation interval between aircraft.

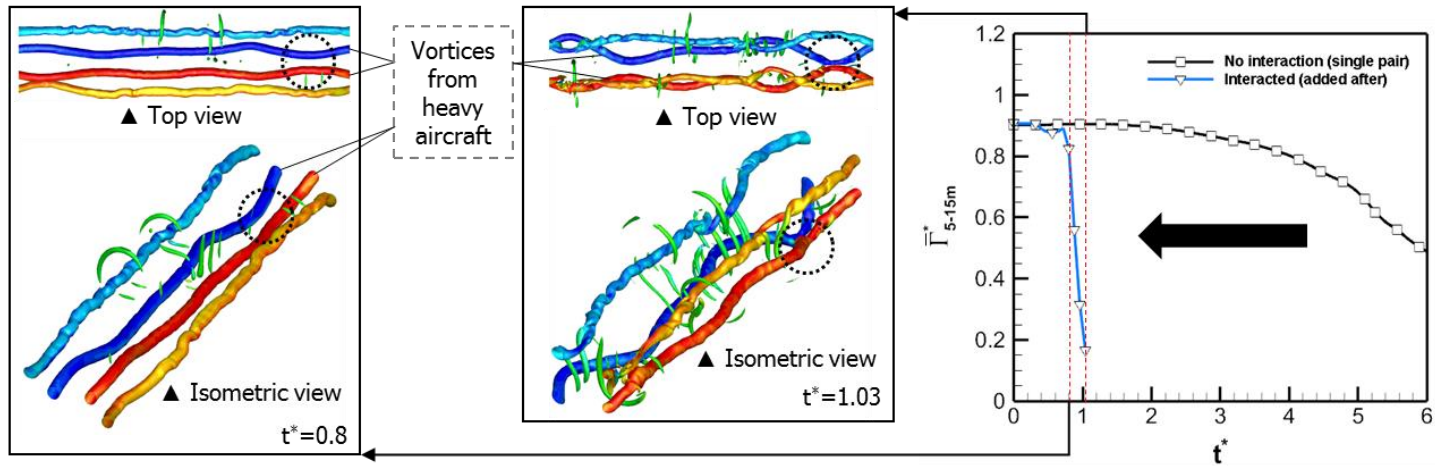


Fig. 17 Top views and isometric views at two different time and averaged circulation of wake vortices of heavy aircraft with respect to t^* interacted with vortices from medium one and without interaction

4. Conclusions

Predicting the behavior of wake vortices is important, because they are not easily dissipated and the circulation strength is strong enough to affect the following aircraft. Among vortices generated from different aircraft, interaction can happen for various reasons such as overlapping routes or due to crosswind. Therefore, it is necessary to investigate the behavior of the wake vortices when those from other aircraft remains in the atmosphere.

In this study, LES simulation has been performed to examine the interaction effect among vortices. The parameters for wake vortices were based on the classification criteria ruled by ICAO. To simulate atmospheric conditions, isotropic turbulence was generated using SNGR and forcing technique. After generating the background turbulence, wake vortices were added to the flow field to investigate the behavior.

The behavior of a pair of wake vortices was found to be dependent on the dimensionless turbulence intensity. In weak turbulence intensity, the linking phenomenon of wake vortices and the formation of a ring caused by the development of Crow instability were evident. On the other hand, irregular distortion due to atmospheric advection was shown in strong turbulence intensity. In addition, the non-dimensional vortex lifespan tends to decrease as the dimensionless turbulence intensity increases, which is consistent with previous research.

In order to investigate the interaction between two pairs of wake vortices, the

vortex parameters were set with respect to the aircraft classification criteria by ICAO. In three cases, which are the combination of 1) light and medium, 2) medium and medium, and 3) medium and heavy aircraft, wake vortices were added to the flow field with time difference and height difference. It was assumed that the wake vortices formed before had been still remained in atmosphere. In all cases, the superposition of the induced effect of each pair of vortices was observed. The upper wake vortices were initially moved toward each other and showed a fast descending speed, while the lower wake vortices were initially spread to both sides and showed a slow descending speed.

It was confirmed that when the upper wake vortices reached the vertical position of lower wake vortices, different results occurred for three cases. In the case of combination light and medium aircraft, the vortices from light aircraft were rapidly dissipated. In addition, as the vortices from light aircraft interacted with the vortices from medium aircraft, a large number of secondary vortices were generated so that the vortex lifespan shortened. In the medium and medium aircraft case, it was confirmed that the circulation intensity temporarily increased due to the combination of the pair of vortices rotating in the same direction. Then the circulation intensity decreased as the linking happened with the vortices rotating in opposite direction. Finally, it was confirmed that the dissipation of wake vortices from heavy aircraft, which interacted with wake vortices from medium aircraft was 5 times faster than the case of a single pair of wake vortices from heavy aircraft without interaction.

Appendix A. Crow Instability Visualization by Han et al. [6]

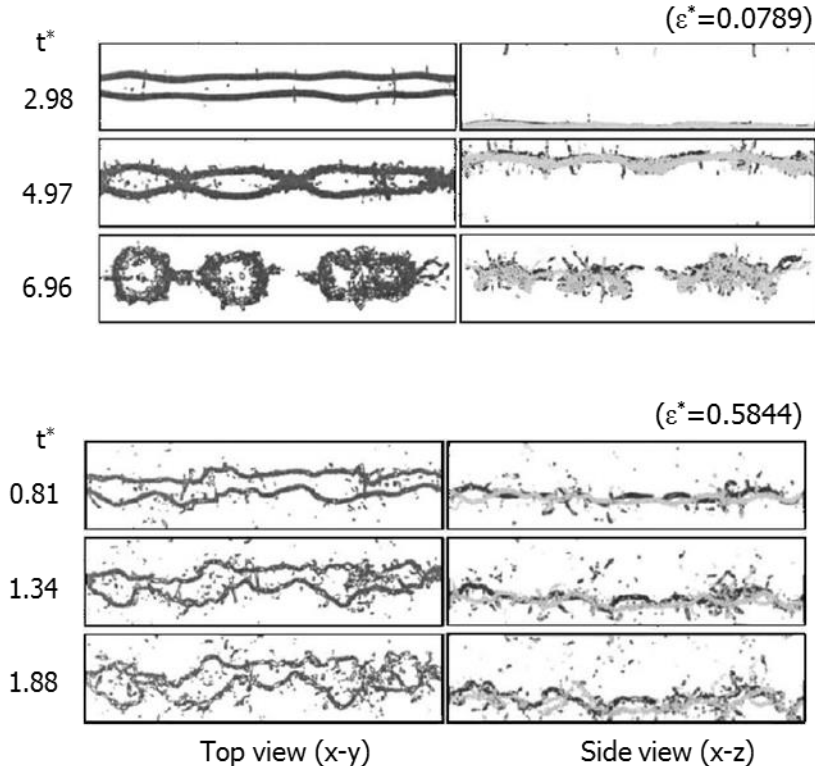


Fig. 18 Top and side views of wake vortices at three different nondimensional times for the case of weak ($\varepsilon^* = 0.0789$) and strong ($\varepsilon^* = 0.5844$) turbulence intensities

Appendix B: The Simplified Model from De Visscher et al. [9]

In the paper of De visscher et al., there is a simplified modeling of wake vortex transport and decay. The modeling of the vortex transport considers the Biot-Savart effect and the stratification as Eq. (16).

$$\frac{dz^*}{dt^*} = v_{BS}^* + v_{str}^* \quad (16)$$

Considering the stratification level as zero, the v_{str}^* term can be ignored so the effect of Biot-Savart, v_{BS}^* can only be in effect as Eq. (14).

In case of the modeling of the vortex circulation decay, De Visscher et al. made an improvement of the model developed by Sarpkaya [22]. Considering the stratification level as zero, the model can be summarized as Eq. (17)

$$\frac{d\Gamma_{tot}^*}{dt^*} = \begin{cases} -\frac{c_1}{t_{d,S}^*} \Gamma_{tot}^* & (if\ t^* \leq t_d^* - \frac{\Delta t^*}{2}) \\ -\frac{c_2}{t_{d,S}^*} \Gamma_{tot}^* & (if\ t^* \geq t_d^* - \frac{\Delta t^*}{2}) \\ \left(\frac{1}{2} \left(\frac{c_2}{t_{\Gamma}^*} + \frac{c_1}{t_{d,S}^*} \right) + \left(\frac{c_2}{t_{\Gamma}^*} - \frac{c_1}{t_{d,S}^*} \right) \frac{t^* - t_d^*}{\Delta t^*} \right) \Gamma_{tot}^* & (otherwise) \end{cases} \quad (17)$$

Here, t_d^* is the starting time of the fast-decay phase. It depends on the

turbulence and since we do not consider the stratification, $t_d^* = t_\Gamma^* = t_{d,S}^*$. $t_{d,S}^*$ is from Sarpkaya's model, and it is computed with respect to ε^* . In addition, there is an interval Δt^* for fitting the results better to the model. It can be a ratio of t_d^* . In other words, $\Delta t^* = \alpha t_d^*$, and α is chosen to be 0.15. The fitting of the model on the present results provides $c_1 = 0.035$, and $c_2 = 1.2$.

References

- [1] D. P. Delisi, and M. J. Pruis, “Estimates of the Initial Vortex Separation Distance, b_0 , of Commercial Aircraft from Pulsed Lidar Data,” 51st AIAA Aerospace Sciences Meeting Including the New Horizons Forum and Aerospace Exposition, Grapevine, Texas, 2013.
- [2] P. R. Veillette, “Data Show That U.S. Wake-turbulence Accidents are Most Frequent at Low Altitude and During Approach and Landing,” Flight Safety Digest, Mar-Apr 2002.
- [3] O’Conner, C. J., and Rtishausser, D. K., “Enhanced Airport Capacity Through Safe, Dynamic, Reductions in Aircraft Separation: NASA’s Aircraft Vortex Spacing System (AVOSS),” NASA/TM-2001-211052.
- [4] V. J. Rossow, “Wake-Vortex Separation Distances When Flight-Path Corridors are Constrained,” Journal of Aircraft, Vol. 33, No. 3, 1996.
- [5] F. Rooseller, and V. Treve, ““RECAT-EU” European Wake Turbulence Categorization and Separation Minima on Approach and Departure,” Eurocontrol, Ed 1.1, 2015.
- [6] J. Han, Y. Lin, D. G. Schowalter, and S. Pal Arya, “Large Eddy Simulation of Aircraft Wake Vortices Within Homogeneous Turbulence: Crow Instability,” AIAA Journal, Vol. 38, No. 2, Feb 2000.
- [7] G. F. Switzer, and F. H. Proctor, “Wake Vortex Prediction Models for Decay and Transport Within Stratified Environments,” 40th Aerospace Sciences Meeting and Exhibit, Reno, Nevada, AIAA Paper 2002-0945, 2002.

- [8] F. H. Proctor, N. Ahmad, G. F. Switzer, and F. M. Limon Duparcmeur, "Three-Phased Wake Vortex Decay," AIAA Atmospheric and Space Environments Conference, Toronto, Ontario Canada, AIAA Paper 2010-7991, 2010.
- [9] I. De Visscher, L. Bricteux, and G. Winckelmans, "Aircraft Vortices in Stably Stratified and Weakly Turbulent Atmospheres: Simulation and Modeling," AIAA Journal, Vol. 51, No. 3, Mar 2013.
- [10] S. C. Crow, "Stability Theory for a Pair of Trailing Vortices," AIAA Journal, Vol. 8, No. 12, 1970.
- [11] M. Van Dyke, "An Album of Fluid Motion," Stanford, California: The Parabolic Press, 1982.
- [12] S. C. Crow, and E. R. Bate, "Lifespan of Trailing Vortices in a Turbulent Atmosphere," AIAA Journal, Vol. 13, No. 7, 1976.
- [13] T. Sarpkaya, and J. J. Daly, "Effect of Ambient Turbulence on Trailing Vortices," Journal of Aircraft, Vol. 24, No. 6, 1987.
- [14] NATS Services, "Aeronautical Information Circular p 001/2015," Civil Aviation Authority, United Kingdom, 2015.
- [15] T. Misaka, T. Ogasawara, S. Obayashi, I. Yamada, and Y. Okuno, "Assimilation Experiment of Lidar Measurements for Wake Turbulence," Journal of Fluid Sciences and Technology, Vol. 3, No. 4, 2008.
- [16] T. Misaka, S. Obayashi, and E. Endo, "Flow Field Reproduction Based on Flight Data Using Numerical Simulation," JSFM 19th Computational Fluid Dynamics Symposium, C5-1, 2005 (in Japanese).

- [17] S. Yamato, and H. Daiguji, "Higher-Order-Accurate Upwind Schemes for Solving the Compressible Euler and Navier-Stokes Equations," *Computer and Fluids*, Vol. 22, No. 2/3, 1993.
- [18] W. Bechara, C. Bailly, and P. Lafon, "Stochastic Approach to Noise Modeling for Free Turbulent Flows," *AIAA Journal*, Vol. 32, No. 3, Mar 1994.
- [19] A. Vincent, and M. Meneguzzi, "The Spatial Structure and Statistical Properties of Homogeneous Turbulence," *Journal of Fluid Mechanics*, Vol. 225, 1991.
- [20] D. C. Burnham, and J. N. Hallock, "Chicago Monostatic Acoustic Vortex Sensing System Volume IV: Wake Vortex Decay," National Technical Information Service, Springfield, Virginia, 1982.
- [21] J. Jeong, and F. Hussain, "On the Identification of a Vortex," *Journal of Fluid Mechanics*, Vol. 285, 1995.
- [22] T. Sarpkaya, "New Model for Vortex Decay in the Atmosphere," *Journal of Aircraft*, Vol. 37, No. 1, 2000.